Korean J. Chem. Eng., 40(11), 2708-2715 (2023)
DOI: 10.1007/s11814-023-1509-9

pISSN: 0256-1115
eISSN: 1975-7220

A novel approach to measuring fluid saturation using X-ray computed tomography

Sobhan Sheikhi†, Alexander Burukhin, and Alexey Cheremisin

Skolkovo Institute of Science and Technology, Moscow, Russia
(*Received 11 December 2022 • Revised 4 June 2023 • Accepted 9 June 2023*)

Abstract−Digital rock analysis using X-ray computer tomography (CT scan) is an ongoing topic for studying the porous media in geothermal, natural gas, and petroleum industries. This study provides a novel approach to calculating fluid saturation in low permeability cores utilizing X-ray computed tomography. In the present study, synthetic low permeability cores were used to analyze two-phase saturation at atmospheric pressure and temperature. In the experiments, no dopant was used for visualizing different phases. As a novelty of the paper, PHREEQC geochemical software was employed to verify the saturation of X-ray CT scanning through modeling the geochemical reaction between aqueous and gaseous phases. This study presents a novel and reliable approach to verify the saturation of X-ray CT scan through geochemical modeling. The results of this study also prove that using the saturation of mass balance as the initial condition of the geochemical modeling leads to an excellent agreement between the saturation of CT scan and geochemical modeling. According to the results obtained, there is a 24% difference between gas saturation in CT scan and mass balance method, while such discrepancy is only 13% between gas saturation in CT scan and geochemical modeling.

Keywords: Saturation, Geochemical Modeling, Cross-section Analysis, CT Scan, Scanning Energies

INTRODUCTION

Porosity and fluids saturations are among the most important parameters for studying fluid flow through porous media. These parameters are crucial in understanding multiphase fluid flow through subsurface porous media in order to manage specific processes, including enhanced oil recovery (EOR), carbon dioxide storage and sequestration, and transport of aqueous contaminants [1]. Different methods have been developed, analyzed, and employed to measure the porosity and saturations, including resistivity method [2,3], radioactive tagging of a fluid [4], radio frequency [5], light absorption [6], and X-ray CT scan [7-10].

X-ray CT scanning and its potential for quantitative analysis of porosity, saturations, and relative permeability in porous material have been presented and reviewed in the literature [11-15]. X-ray CT scan is a nondestructive technique for taking images from internal sections of porous material. This approach can be used to describe the microscopic pore structure of different materials and observe the single and multiphase fluid flow in porous media. In geothermal, natural gas, and petroleum industries, X-ray CT method can be utilized for the purpose of discovering vugs and fractures in the core scale, measuring the porosity and bulk density, and observing the fluids saturation during multiphase core flooding experiments [16,17].

Hicks et al. [18] demonstrated the limitations and feasibility of X-ray CT for measuring fluids saturations in three dimensions in carbonate cores during the flooding operation [18]. They reported porosity and residual oil saturation distribution of the cores. Using the same technique, Brancolini et al. [19] determined the porosity variation in a poorly consolidated sandstone and reported a linear relationship between CT number and porosity [19]. Durand [20] combined X-ray CT technique and local resistivity method to measure the fluid distribution in a core during steady state and unsteady state conditions [20]. Olivier et al. [21] performed X-ray CT tests to analyze the flow behavior in vuggy carbonate rocks [21]. Alshehri et al. [22] monitored fluid saturation in fractured porous media using X-ray CT approach during the imbibition [22]. Kusanagi et al. [23] developed a new numerical method based on extracted data from X-ray CT to analyze the fluid flow through different vuggy porous media [23]. Using CT scans, Moghadasi et al. [24] investigated the multiphase relative permeability in a sand-pack and a Berea sandstone [24]. Local saturatio in different cross sections of the sample can be measured through applying X-Ray CT technique. Wang et al. [17] determined petrophysical properties of a natural fractured porous media by X-ray computed tomography [17]. Alhosani et al. [25] employed X-ray micro-tomography to study in situ three-phase gas injection in a natural porous media at elevated temperature and pressure [25].

The difference in attenuation coefficients of different materials is the key for recognizing the various fluids by X-ray CT scan. Some of the fluids in porous media have very close attenuation coefficients. Hence, dopants are used to make difference in attenuation coefficients and increase the efficiency of the CT scan method through calculating the fluids saturations [26-28]. Considering such limitation in CT scan approach, there is a tendency to use other approaches to verify the saturation obtained by CT scan. Generally, material balance is used to verify the saturation of a CT scan approach. However, the material balance is related to the initial condition of the porous media, and due to the equilibrium of different phases, the saturation is changing slightly, which affects the

†To whom correspondence should be addressed.
E-mail: sobhan.sheikhi@skoltech.ru

ultimate saturation of fluids. As the novelty in this work, PHREEQC geochemical modeling has been presented as a reliable approach for modeling the equilibrium in porous media and verifying the fluid saturation obtained using CT scan method. Besides, a faster and a more simplified method has been utilized to calculate the porosity and saturation with X-ray CT scan, which is based on only two scanning steps. Static two-phase experiments were performed to confirm the ability of the proposed approach in analyzing fluid saturations in synthetic porous media. The contents of the paper are as follows: Section 2 describes the experimental methodology, and section 3 presents the modeling approach. Results and discussion are presented in section 4, and the fifth section concludes the paper.

EXPERIMENTAL METHODOLOGY

1. Material

In the present study, static experiments were performed in artificial cores with air as the gaseous phase and distilled water as the aqueous phase. In the following section, the preparation steps of the artificial cores and fluids of the porous medium are described in detail.

1-1. Preparation of Artificial Cores

In order to make the low permeability porous media (as low as possible), the finest available glass beads (1-50 micrometer diameter) were selected to prepare the artificial cores. An actual core is formed by particles joined together with cement. The general structure of the artificial core is very similar to that of the real core in that concern. The bonding of particles in an artificial core formed by glass bead particles is formed by partial fusion of particles. Artificial cores are widely used for investigation when the well-defined condition of core properties is required. Small containers (150 ml) were chosen to sinter the glass beads inside them. The temperature of the oven was set at 695 °C. Note that during the sintering procedure, after containers were filled with glass beads, the sample was put into the oven at the ambient condition, then the above-mentioned temperature was set. It took about an hour to reach the desired temperature.

The sample was cooled gradually inside the oven after 2 hours staying on 695 °C. The sample was not completely impermeable but did not crack. A coring machine was utilized to cut the sample into the desired dimensions. Porosity and permeability of the sample were then measured with nitrogen gas and water. The porosity and liquid permeability were reported as 0.124 and 142 mD, respectively. Also, the length of the core sample was 50 mm and its diameter was 29 mm. The upper side of the core samples was directly exposed to the hot air, while the lower side received indirect heat. This makes a porosity-permeability difference along the core which will be captured using CT scan analysis and explained in section 5.1.

1-2. Fluids

As mentioned, in this study air and deionized water were used as gaseous and aqueous phases, respectively. It is required to have the composition of the gas phase as it can interact with the distilled water in the studied porous media. Table 1 shows the composition of air used in this study. Since the exact density of the aqueous phase is required to calculate the water saturation (in mass balance), the density of the water phase was measured by densitometer, which shows the value of 1 g/cc--exactly the same density from the literature.

Table 1. Composition of the air in the laboratory

Gas species	N_2	O_2	H_2O	CO_2
Mole fraction%	77	19	3.96	0.04

2. Experiments

2-1. Using CT Scan for Measurement of Saturations

According to the literature, a standard method is used to measure the porosity and saturations using CT scan images. The standard method for porosity and two phase saturation measurement is as follows:

1. Scanning dry core in a certain energy (first reference scan).
2. Fully saturating the core with water.
3. Scanning fully saturated core with the same energy: porosity along the core is calculated in this step (second reference scan).
4. Displacing water in the pores by air: Draining specific amount of water by air to reach two phases saturation in the core.
5. Scanning core with the same energy: two-phase saturation along the core is calculated following this step.

The standard method cannot be used for low permeability systems, as it is not possible to fully saturate the core with water phase in the second step. Thus, since the porosity and permeability of the tight cores are too low, reaching fully saturated core with a liquid phase is almost impossible. Hence, it is required to use a modified method for low permeable cores.

In the present section, the modified method procedure for calculating porosity and saturation is presented. In this method, there is no need to fully saturate the core with the second phase for the second reference scan. The modified method for two phase (air-water) saturation measurements is as follows:

1. Scanning dry core in one energy. Porosity along the core is calculated in this step.
2. Displacing specific amount of air by water and imbibing specific amount of water to reach two phases saturation inside the core.
3. Scanning the core in same energy: two-phase (distilled water/air) saturation is calculated after this scan.

Considering the procedure of the modified method, two steps are eliminated in comparison to the standard method. These changes omit one challenging step and facilitate the experimental procedure. Looking at the calculation process in the standard method, it can be noted that in the standard procedure, the data from two reference scans are used to calculate the porosity, and consequently, the two-phase saturations. In contrast, in the modified procedure, the porosity of each slice is calculated directly from the first scan (dry core). By decreasing the experimental steps and doing the calculations directly from one scan, inevitable systematic errors can be reduced. These errors may occur in any experimental steps including core saturation and changing the condition of scanner elements such as its source and receiver. In the standard procedure, each of the two reference scans leads to separate systematical errors, and using them together in calculation leads to merging such errors and an increase in sporadic errors.

2-2. Procedure of the Experiments

CT scan images were provided using the GE Phoenix industrial CT scanner (v|tome|x L 240/180) with two X-Ray tubes: 1) Micro-focused for lower resolution scans which allows to work with large samples (up to 800 mm diameter, 1,300 mm length, 50 kg), working with 240 kV accelerating voltage and up to 320 W power. 2) Nano-focused tube with transmission design capable of working with submicrometer focal spot size, which provides scans with resolution below one μm with accelerating voltage up to 180 kV, and power up to 20 W. The detector is the DXR250 photodiode array with scintillator, 2024×2024 pixels with pixel size 0.2×0.2 mm. The scans were performed with a nano-focused tube as a high resolution is required. Before the scanning, detector and X-ray tube were calibrated for darkfield and 2-3 light fields.

CT scanning was performed for two energy values of 80 kV and 120 kV with two currents of 300 μA and 200 μA, respectively. The ratio of the distance from source to detector (800 mm) and to sample (66 mm) provided resolution of 16.5 μm/voxel. The exposure time was 500 ms and the final projection image was an average of three consequent pictures. It must be highlighted that no filters were used and the full scan of 2400 projection was processed with Phoenix Datos 2 reconstruction software for reconstructing the 3D image. CT images were taken at atmospheric pressure and ambient temperature (25 °C).

After preparing the cores, they were evacuated for at least 2 hrs and kept in 15 MPa pressure of distilled water for another 2 hrs. Using saturator apparatus, the saturation of water and air inside the core reached 90.1 and 9.9 percent (using mass balance), respectively. Regarding higher relative permeability of air and low permeability of the porous media, the aqueous phase was not able to completely push the gas outside of the core. Therefore, a certain amount of air remained in the core and was introduced as the second phase (gas phase). The injection process was finished after 100 min in a constant pressure. Then, the core was put into the distilled water and rested to gain equilibrium between gaseous and aqueous phases. After two days, CT scan images were taken and used for the porosity and saturation analysis. Mass balance and pore volume of the core samples were also used for estimating the amount of each phase.

MODELING PROCEDURE

PHREEQC software was used to simulate air-water interactions in the studied porous media. PHREEQC is a famous geochemical software for modeling the geochemical reactions between gaseous, aqueous, and solid phases. PHREEQC applies the Peng-Robinson equation of state for estimating the solubility of gases at high pressures [29]. In this software, the equilibrium condition is calculated by solving the mass action equations [29,30], which leads to the minimum Gibbs free energy [31].

The main reason for using geochemical modeling origiinates from the idea that the volume (saturation) of the gaseous phase can change due to the gas-water interaction. Regarding the material of the porous media (glass beads), geochemical reactions between aqueous and solid phases were neglected in the modeling. However, the reactions between gaseous and aqueous phases are important as the air components can dissolve into the distilled water during the equilibrium process (two days imbibition).

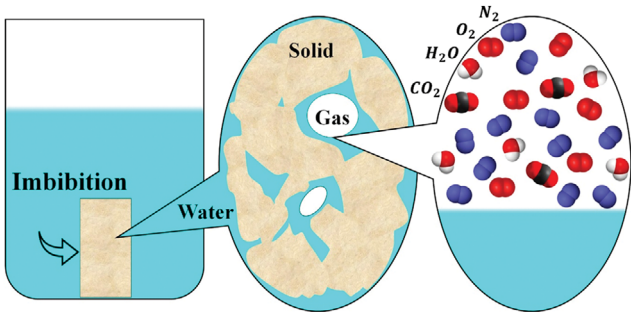

Fig. 1. Different phases in the studied case.

A static batch interaction model was selected to simulate the gas-brine interaction system. It is assumed that pressure and temperature of the system are constant, but the volume of the gas phase is variable. The amount of the injected water (from mass balance) was selected as the initial condition for the static gas-water interaction system.

The volume and saturation of the gaseous phase can change due to the solubility of the air components in the aqueous phase after the air-water equilibrium. In PHREEQC geochemical package, the solubility of the i^{th} gas specie (m_i) is estimated using the following equation [29]:

$$m_i = K\frac{\varphi_i P_i}{\gamma_i} \quad (1)$$

In Eq. (1), K is the equilibrium constant, φ_i is the fugacity factor, P_i is the partial pressure, and γ_i is the activity coefficient in the aqueous phase. PHREEQC measures the fugacity coefficient (activity coefficient in the gaseous phase) using the Peng-Robinson equation of state [29,32]. However, in the low-pressure systems (<10 atm), the fugacity coefficient is close to 1, but it can be ignored in calculations of the solubility. Fig. 1 illustrates different phases in the studied case during the equilibrium.

CT IMAGE ANALYSIS

Various image processing codes and applications can be used to analyze the CT scan images and recognize the porosity and saturation of different phases. In the present study, ImageJ software was employed in order to analyze CT images. Using ImageJ, the software can automatically segment different materials in the image based on their grayscale values.

Regarding the images of this study, grayscale values of the cross-sectional 2D CT images were used to analyze different phases in the porous media. Each image was saved in a 16-bit grayscale type. Generally, higher attenuation coefficient leads to less signal detection and lighter color (higher value of the voxel). Grayscale value of each pixel depends on the attenuation coefficient of the material. Also, at a specific temperature, pressure, and scanning energy, each material has a particular attenuation coefficient.

The grayscales values depend on the attenuation coefficients but differ in each scan. For example, in the same condition, the grayscale value of air in one scan might be 2000, whereas in another

scan, it might be 4200. Therefore, it is required to normalize these grayscales to have a particular quantity for each material in a constant condition. Normalizing the grayscales requires two reference fluids. Since the air usually has the lowest grayscale value, it was selected as the first reference, and its values were shifted to zero. Water was chosen as the second reference to normalize the linear changes in pixel value and attenuation coefficient. The normalized number is named CT number and should be almost constant for a particular material in different scans under the same condition. Thus, the following equation can be presented to calculate the CT number of material x (CT_x):

$$CT_x = -1{,}000\frac{GS_w - GS_x}{GS_w - GS_a} \quad (2)$$

where, GS_x is the calculated grayscale value of the material x, GS_a is the grayscale value of air, and GS_w is the grayscale value of water. During normalization, CT numbers of air and water are always constant and equal to −1,000 and 0, respectively. Different cross-section areas can be selected for calculating porosity and saturations. The method used for selecting cross-section area will be explained in section 5.1. However, the porosity of each slice can be calculated as follows:

$$CT_{dry} = CT_m(1-\varphi) + \varphi CT_a \quad (3)$$

In Eq. (3), CT_{dry} is the CT number of the dry medium, CT_m is the matrix CT number, CT_a is the air CT number, and φ is the porosity. Matrix CT number is calculated using the mode grayscale value of each slice. Mode value shows the most common grayscale value in each slice. Since about 90 percent of the core space is occupied by matrix, the mode value represents the grayscale value of matrix. The CT number of the dry cores is calculated from the mean grayscale value in each slice. Saturation of the water and gas phases can be obtained using the following equations:

$$CT_{2-phase} = (1-\varphi)CT_m + \varphi S_w CT_w + \varphi S_g CT_g \quad (4)$$

$$S_g + S_w = 1 \quad (5)$$

where, $CT_{2-phase}$ is the two-phase CT number, CT_w is the water CT number, S_g is the gas saturation, and S_w is the water saturation.

RESULTS AND DISCUSSION

In the present section, first, the porosity of the studied porous medium is analyzed with respect to the hardening effect. Regarding the results of section 5.1, a suitable cross-section area was selected for saturation analysis. In section 5.2, the saturation of different phases is analyzed and compared with the saturation of the mass balance. Saturations of CT scan are verified by the geochemical modeling in section 5.3.

1. Porosity Analysis and Hardening Effect

Using nitrogen in gas pycnometry, the porosity of the studied cores is calculated as 0.124. In addition, the porosity of the studied porous media can be calculated from CT scan images. Results of the image processing reveal that the porosity obtained from CT scan images strongly depends on area of the analyzed cross-section, which is caused by beam hardening effect.

Beer's law, which is the basis of the reconstruction algorithm in CT instruments, must be utilized only for monochromatic X-rays, while polychromatic X-rays result in the beam hardening effect. This problem causes the X-ray energy spectrum variation through the object. In the cylindrical geometry, all the projections are similar. However, according to the beam hardening effect, the low energy part of the X-ray beam attenuates on closest to X-ray tube part of the core. Therefore, the outer border of the sample seems to be denser than the inner part. Beam hardening is more intensive in dense and low perm objects (such as formation rocks) than in light materials (such as human tissue). Some software packages corrections and filtering X-ray sources could be used to alleviate the beam hardening effect [33]. However, both of them are not always usable and accurate enough. More details can be found in Van Geet et al. [33].

Fig. 2 represents the normalized grayscale values of a single line in a cross-section of the studied case with respect to the energy of scanning (80 kV and 120 kV). The data are normalized to the maximum grayscale value of the image for each energy. As shown in Fig. 2, gradual change of grayscale from the outer boundary of core to the center is more significant in the lower energy (80 kV). The pixels under the plotted single line can represent either the matrix or the pores; therefore, the data show high fluctuation in some areas in Fig. 2. Thus, the average grayscale value reduces more while it

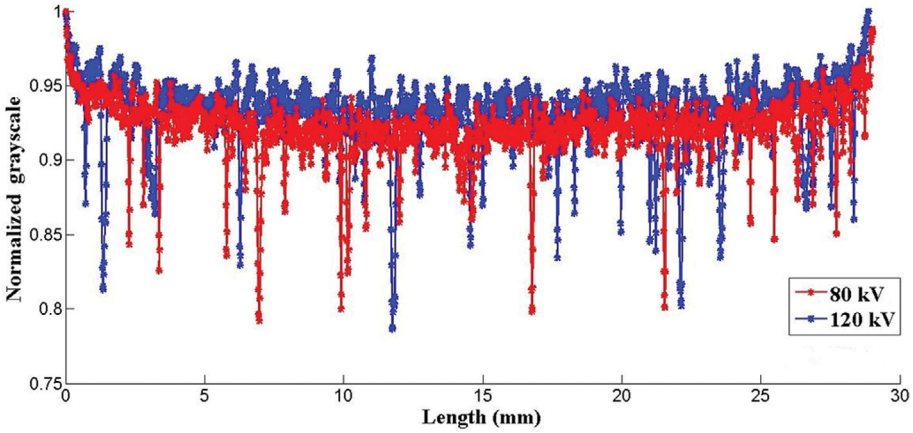

Fig. 2. Normalized grayscale values of a single line in a cross-section of the studied case.

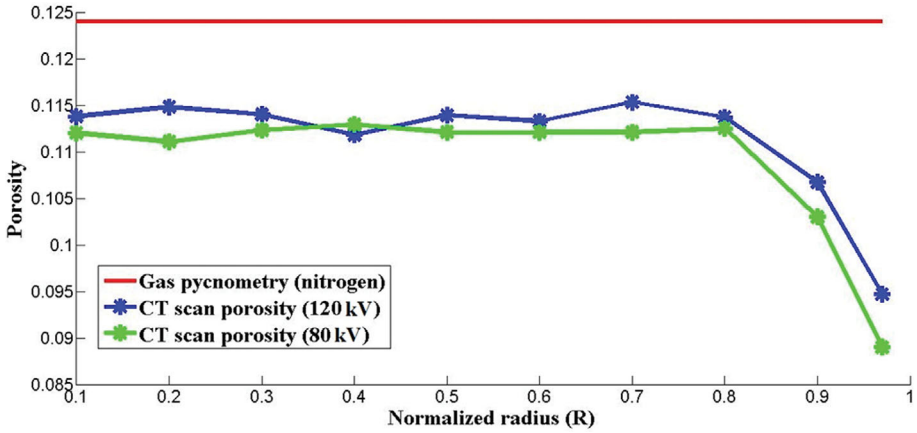

Fig. 3. Porosity of the studied case achieved from CT scan with respect to the radius of the cross-section.

goes toward the center in the lower energy scanning. Hence, scanning in the lower energy causes a more intensive beam hardening effect and influences the data, which can lead to a higher error in calculations.

In the present study, a sensitivity analysis was performed to find the area of the sample affected by beam hardening. The radius of the selected area must be chosen a little smaller than the radius of the core. Fig. 3 demonstrates the porosity of the studied case with respect to the radius of the cross-section.The maximum radius of the analyzed area is normalized to the maximum radius of the core. Regarding Fig. 3, there is a proper agreement between experimental porosity (achieved from gas pycnometry) and CT scan porosity when the radius of the analysis is between 0.1r and 0.8r (~4% difference). However, gas pycnometry shows a higher porosity as

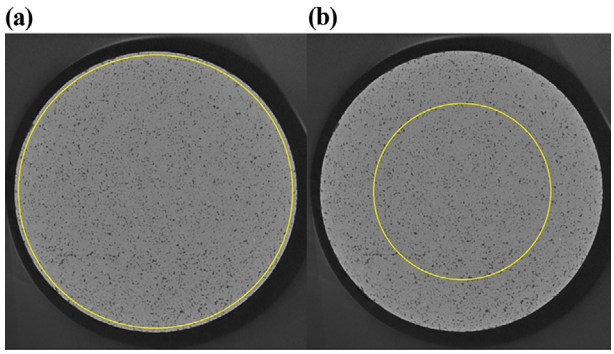

Fig. 4. Cross-sections for calculation of saturation and porosity: yellow ovals, (a) maximum cross section: 0.97R, (b) selected cross section: 0.6R. R=14.5 mm.

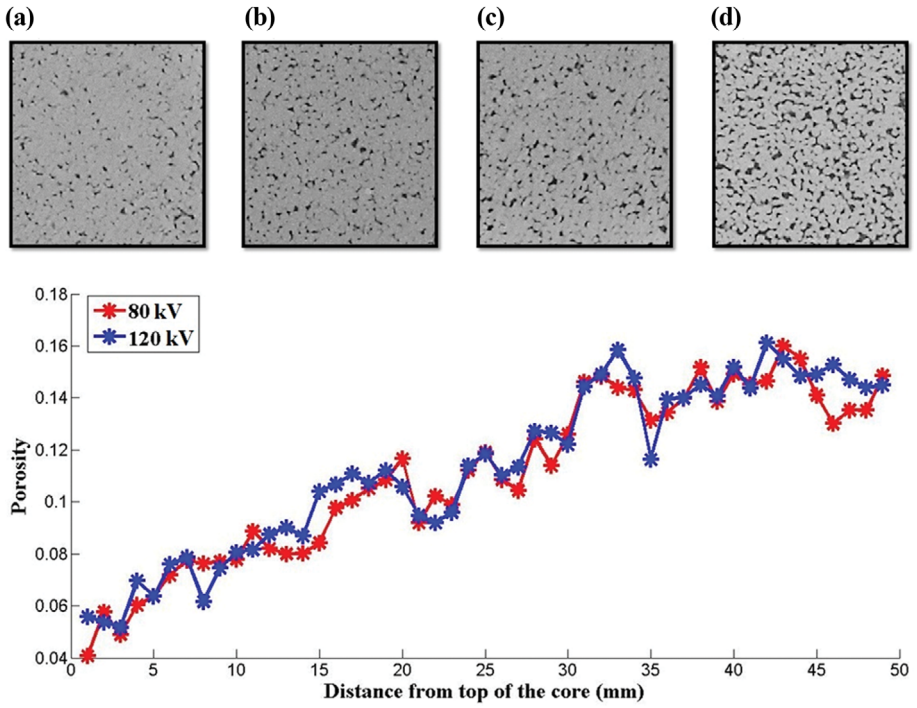

Fig. 5. Porosity along the studied core for 80 kV and 120 kV energies, (a) distance=5 mm, (b) distance=20 mm, (c) distance=30 mm, (d) distance=45 mm.

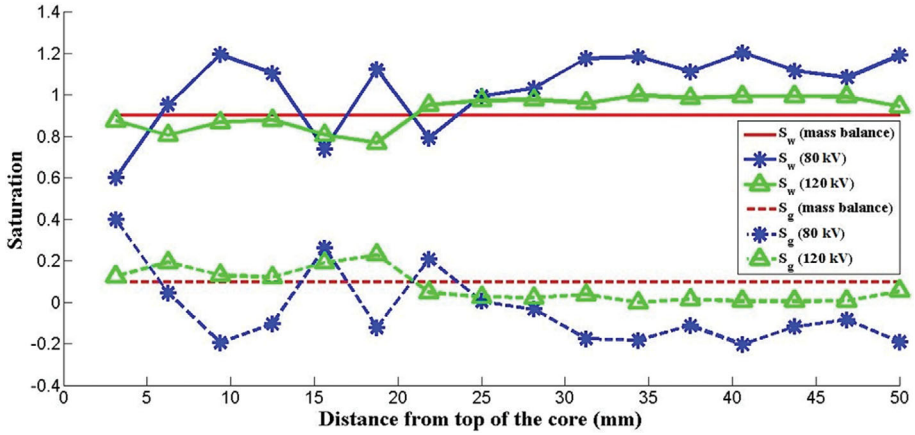

Fig. 6. Saturation along the core sample for 80 kV and 120 kV X-ray scanning energies.

nitrogen molecules can easily transport to some nano-scale pores that cannot be observed in CT scan images. Fig. 3 also shows that using 80 kV energy leads to a higher disagreement between gas pycnometry porosity and CT scan porosity. In summary, using the lower energy magnifies the beam hardening effect and causes higher error. By applying higher energy, better accuracy can be achieved. Considering the impact of beam hardening, radius=0.6R was selected for saturation analysis in the studied case. Fig. 4 gives more information about the maximum and selected cross-section area used for cross-section analysis.

Fig. 5 presents the porosity of porous medium along the studied core with the scan energy of 80 kV and 120 kV. In both analyzed energy values, the porosity of the second half-length of core sample (right side) is higher than the porosity of the first half-length (left side). Fig. 5 also contains the CT scan images from different cross-sections of the core. As these CT images show, the second half-length of core has larger pores, and the first half-length of core sample contains narrower pores.

2. Analyzing the Saturations of Different Phases

In the present section, saturations of the water and gas phases in the studied core sample are analyzed in detail. Fig. 6 represents the measured saturation profiles along the sample core with 80 kV and 120 kV energies. As it is shown in Fig. 6, X-ray energy of 120 kV results in more logical saturation, because most of the calculated saturations in different cross-sections are in the acceptable physical range (between 0 to 1). In contrast, X-ray energy of 80 kV does not provide sensible saturation as the calculated saturations are negative in some of the cross-sections.

Table 2 represents the average saturation of water and gas phases obtained from mass balance and CT images. Considering Table 2, the average saturation of water and gas achieved from the mass blalace is 0.9 and 0.1, respectively. The average values of water and gas saturation estimated from scan energy of 80 kV are 1.1263 and −0.127, while in the scan energy of 120 kV, values of water and gas saturation are 0.924 and 0.076, respectively. According to the literature, for X-ray energy above 100 kV, the impact of the effective atomic number on the CT images disappears, and the grayscale of CT image is proportional to the bulk density [16]. As it can be seen from the results of figures and tables, saturation measurements show

Table 2. Average saturation of water and gas phases achieved from mass balance and CT images

Saturation		S_w	S_g
Mass balance		0.9	0.1
120 kV	Saturations	0.924	0.076
	Relative error	2.6%	24%
80 kV	Saturations	1.0378	−0.038
	Relative error	15.3%	138%

better accuracy when higher energy method is applied. It can be concluded that when the applied energy is higher, more penetration occurs, leading to less contrast and less sensitivity to fluids in porous media. As a result, it seems that there is a higher accuracy when a high scanning energy is employed.

Fig. 6 also shows that by applying higher energy values, water and gas saturations highly fluctuate in the first half-length of the core. On the other side, saturations are almost constant (uniform) in the second half-length of the core. Higher fluctuation (saturation heterogeneity) in the first half-length of the core has been created due to the lower porosity and permeability in this section of the core (see Fig. 5). Lower porosity and permeability (smaller pore size and geometry) trap the gas bubbles in narrow throats (due to capillary force) and do not allow them to move. In the section with higher porosity and permeability, gas bubbles easily move, which culminates in a uniform saturation.

3. Calculating Saturation by Geochemical Modeling

As distilled water is injected into the studied porous medium, it can interact with the gas phase through dissolution of the gas components. Dissolution of the gas components can reduce the volume (saturation) of the gas phase. Therefore, mass balance saturation is different from the CT scan saturation. In this section, PHREEQC batch geochemical modeling has been applied as a reliable tool for estimating the reactions inside the studied porous medium. For this purpose, the saturation obtained from material balance was selected as the initial condition of the geochemical model, expressing 0.111 liter gas per 1 kg water. The results of the modeling prove that all

Table 3. Amount of gas dissolution per 1 kg water

Gas species	N_2	O_2	H_2O	CO_2
Dissolution (mole/lit)	−1.00e-03	−9.08e-04	−5.79e-05	−8.46e-05

Table 4. Saturation of water and gas phases achieved from modeling and 120 kV CT scan

Saturation	S_w	S_g
Modeling	0.933	0.067
120 kV	0.924	0.076
Relative error	1%	13%
Absolute error	0.9%	0.9%

of the gas components (N_2, O_2, H_2O, and CO_2) are dissolved in the aqueous phase. After equilibrium, the amount of remaining gas is 0.0718 liter per 1 kg water. Table 3 represents the amount of gas dissolution per 1 kg water in the studied case.

In the previous section (5.2), it was shown that 80 kV scan energy does not provide sensible results for the studied case. Hence, only 120 kV scan energy has been compared with the saturations of the geochemical modeling. Table 4 presents the saturation of water and gas phases achieved from the geochemical modeling and CT images. Regarding Table 4, average saturation of water and gas obtained from the modeling was 0.933 and 0.067, respectively. These values are close to the average saturation of CT images (0.924 and 0.76), as the difference (error) is less than 13%.

Fig. 7 presents a comparison between three methods that were used to estimate the average saturations (mass balance, geochemical modeling, and CT scan). Regarding Fig. 7, there is a higher similarity between the saturations of CT scan and geochemical modeling for both water and gas phases. The relative error of gas saturation is 24% for the comparison between CT scan and mass balance. In contrast, by comparing CT scan and geochemical modeling, the relative error is 13% resulted (see Tables 2 and 4).

SUMMARY AND CONCLUSIONS

By coupling X-ray computed tomography and PHREEQC geochemical modeling, a novel approach is presented for the measurement of fluid saturations in the low permeable cores. No dopant was used to clarify different phases in the experiments. Synthetic cores were used to analyze two-phase saturations at atmospheric pressure and temperature. In the proposed approach, the saturations of mass balance were used as the initial condition for the geochemical modeling, and fluid saturations were calculated through modeling the reactions between aqueous and gaseous phases. An appropriate agreement was obtained between the saturations of geochemical modeling and CT scan. The main conclusions of this study are elaborated below:

- Using the modified CT scan method, although the number of scanning steps was reduced, sensible results were obtained for both porosity and saturations.
- Due to the hardening effect, it is required to select a smaller radius for analyzing the porosity and saturations (<0.8R).
- Both 80 kV and 120 kV scanning energies can estimate the porosity of the medium properly. However, the saturations corresponding to 120 kV scanning energy were more accurate.
- Saturations of water and gas phases follow the porosity and permeability of the porous medium as there is higher saturation heterogeneity in low permeable sections of the core.
- Saturations of the mass balance method do not match the saturations of CT scan as it cannot predict the gas-water equilibrium inside the core.
- Saturations of the mass balance should be selected as the initial condition of the geochemical modeling.
- There is a higher agreement between geochemical modeling and CT scan approach because the geochemical modeling shows that gas dissolution occurs during the equilibrium in the studied porous medium.

LIST OF SYMBOLS

CT_i : CT number of the i^{th} material
GS_i : grayscale value of the i^{th} material
K : equilibrium constant
m : solubility of the gas [mole/lit]
P : partial pressure of the gas [atm]
R : normalized radius of the core [r/r_{core}]
S_g : saturation of the gas phase

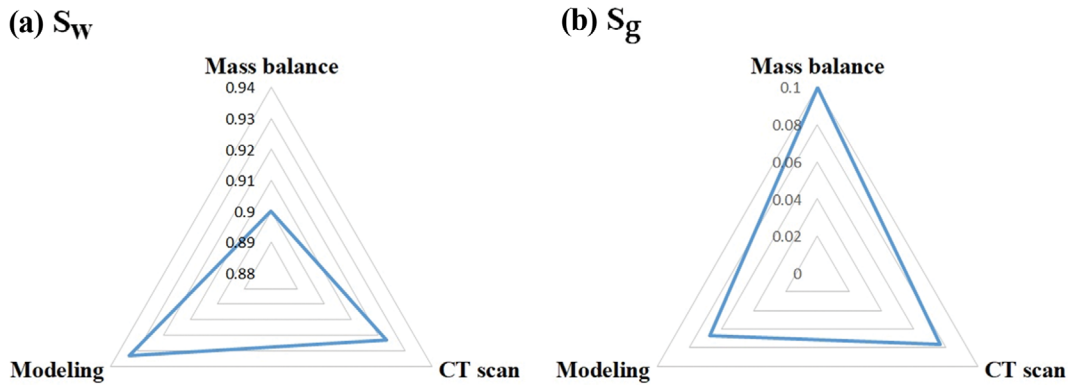

Fig. 7. Water and gas saturations achieved from mass balance, geochemical modeling, and CT scan.

S_w : saturation of the water phase
γ : activity coefficient in the aqueous phase
φ : porosity of the medium

REFERENCES

1. N. Kampman, M. Bickle, M. Wigley and B. Dubacq, *Chem. Geol.*, **369**, 22 (2014).
2. G. De Josselin de Jong, *Eos, Trans. Am. Geophys. Union*, **39**(1), 67 (1958).
3. Z. Liu and S. M. Moysey, *ISRN Geophys.*, **2012** (2012).
4. M. J. Beran, *Summary of dispersion of soluble matter in slowly moving fluids*, Harvard University (1955).
5. G. Round, *Nature*, **188**(4747), 305 (1960).
6. E. Deutsch, *Nature*, **185**(4714), 675 (1960).
7. A. Laird and J. Putnam, *J. Pet. Technol.*, **3**(10), 275 (1951).
8. E. Chavez Panduro, M. Torsæter, K. Gawel, R. Bjørge, A. Gibaud, Y. Yang, S. Bruns, Y. Zheng, H. Sørensen and D. Breiby, *Environ. Sci. Technol.*, **51**(16), 9344 (2017).
9. A. M. Alhammadi, Y. Gao, T. Akai, M. J. Blunt and B. Bijeljic, *Fuel*, **268**, 117018 (2020).
10. Y. Yang, L. Tao, S. Iglauer, S. H. Hejazi, J. Yao, W. Zhang and K. Zhang, *Energy Fuels*, **34**(9), 10762 (2020).
11. L. Salvo, P. Cloetens, E. Maire, S. Zabler, J. J. Blandin, J.-Y. Buffiere, W. Ludwig, E. Boller, D. Bellet and C. Josserond, *Nucl. Instrum. Methods Phys. Res. Sect. B-Beam Interact. Mater. Atoms*, **200**, 273 (2003).
12. E. Maire and P. J. Withers, *Int. Mater. Rev.*, **59**(1), 1 (2014).
13. A. Du Plessis, B. J. Olawuyi, W. P. Boshoff and S. G. Le Roux, *Mater. Struct.*, **49**(1-2), 553 (2016).
14. H. Menke, C. Reynolds, M. Andrew, J. P. Nunes, B. Bijeljic and M. Blunt, *Chem. Geol.*, **481**, 27 (2018).
15. A. Shabani, M. B. Shahparast and F. Barzegar, *Energy Sources Part A-Recovery Util. Environ. Eff.*, 1 (2020).
16. S. Akin and A. Kovscek, *Geological Soc. Publications*, **215**(1), 23 (2003).
17. F. Wang, Y. Li, X. Tang, J. Chen and W. Gao, *J. Nat. Gas Sci. Eng.*, **28**, 215 (2016).
18. P. J. Hicks Jr, R. Narayanan and H. A. Deans, *SPE Form. Eval.*, **9**(01), 55 (1994).
19. A. Brancolini, I. Mackenziei, F. Radaelli and F. Rossi, *X-ray CT evaluation of poorly consolidated, thin-bedded core*. SPWLA 36th Annual Logging Symposium, Society of Petrophysicists and Well-Log Analysts (1995).
20. C. Durand, *Combined use of X-ray CT scan and local resistivity measurements: A new approach to fluid distribution description in cores*, SPE Annual Technical Conference and Exhibition, Society of Petroleum Engineers (2003).
21. P. Olivier, L. Cantegrel-Gassiot, J. Laveissiere and N. Guillonneau, *Petrophysics*, **46**(06) (2005).
22. A. J. Alshehri and A. R. Kovscek, *An X-ray CT study of multidimensional imbibition in dual porosity carbonates*, SPE Annual Technical Conference and Exhibition, Society of Petroleum Engineers (2012).
23. H. Kusanagi, N. Watanabe, T. Shimazu, M. Yagi, T. Komai and N. Tsuchiya, *X-ray CT based numerical analysis for fluid flows through vuggy carbonate cores*, 20th Formation Evaluation Symposium of Japan, Society of Petrophysicists and Well-Log Analysts (2014).
24. L. Moghadasi, A. Guadagnini, F. Inzoli, M. Bartosek and D. Renna, *J. Pet. Sci. Eng.*, **145**, 453 (2016).
25. A. Alhosani, A. Scanziani, Q. Lin, Z. Pan, B. Bijeljic and M. J. Blunt, *Adv. Water Resour.*, **134**, 103432 (2019).
26. L. Weifeng, L. Qingjie, Z. Zhang, M. Desheng, W. Kangyun and L. Zhenpeng, *Pet. Explor. Dev.*, **39**(6), 758 (2012).
27. K. Alshibli and Z. A. Jarrar, *Geotechnical Testing J.*, **44**(4) (2020).
28. N. K. Jha, M. Lebedev, S. Iglauer, M. Ali, H. Roshan, A. Barifcani, J. S. Sangwai and M. Sarmadivaleh, *J. Colloid Interface Sci.*, **562**, 370 (2020).
29. D. L. Parkhurst and C. Appelo, Description of input and examples for PHREEQC version 3: a computer program for speciation, batch-reaction, one-dimensional transport, and inverse geochemical calculations, US Geological Survey (2013).
30. D. L. Parkhurst and C. Appelo, USER'S GUIDE TO PHREEQC (VERSION 2) (Equations on which the program is based), Technical report, US Geological Survey (1999).
31. Y. Zou, C. Zheng and S. Sheikhi, *Chem. Geol.*, **559**, 119992 (2020).
32. D.-Y. Peng and D. B. Robinson, *Ind. Eng. Chem. Fundam.*, **15**(1), 59 (1976).
33. M. Van Geet, R. Swennen and M. Wevers, *Sedimentary Geol.*, **132**(1-2), 25 (2000).